Check for updates

The influence of composition on the functionality of hybrid CuO–ZnO–Al$_2$O$_3$/HZSM-5 for the synthesis of DME from CO$_2$ hydrogenation

Yubing Hu, Yajing Zhang, [ID] * Jie Du, Chunyan Li, Kangjun Wang,* Lidong Liu, Xinrui Yu, Kai Wang and Nan Liu

A series of CuO–ZnO–Al$_2$O$_3$/HZSM-5 hybrid catalysts with different Cu/Zn ratios and disparate Al$_2$O$_3$ doping were prepared and characterized by XRD, BET, H$_2$-TPR, NH$_3$-TPD and XPS techniques. The optimal Cu/Zn ratio is 7 : 3, and the introduction of a suitable amount of Al$_2$O$_3$ to form hybrid catalysts increased the BET specific area and micropore volume, facilitated the CuO dispersion, decreased the CuO crystallite size, increased the interaction between CuO and ZnO, enhanced the number of weak acid sites, altered the copper chemical state and improved the catalytic performance consequently. The highest CO$_2$ conversion, DME selectivity and DME yield of 27.3%, 67.1% and 18.3%, respectively, were observed over the CZA$_7$H catalyst. The suitable temperature of 260 °C and the appropriate space velocity of 1500 h^{-1} for one-step synthesis of dimethyl ether (DME) from carbon dioxide (CO$_2$) hydrogenation were also investigated. The 50 h stability of the CZA$_7$H catalyst was also tested.

1. Introduction

CO$_2$ emission is increasing at an unparalleled rate due to fossil fuel combustion in recent years.[1] As a consequence, excessive CO$_2$ release leads to a series of problems such as global warming and environmental pollution.[2,3] Therefore, CO$_2$ recycling and utilization are very imperative.[4,5] CO$_2$ hydrogenation to dimethyl ether (DME) is an excellent option.[6]

DME is attracting more and more interest as a green fuel because it produces less CO$_x$, NO$_x$, and SO$_x$ particulates when combusted.[7] Therefore, DME is considered as a potential environmentally friendly alternative option to petrol diesel for diesel engines.[8] Meanwhile, DME, as a vital chemical intermediate, can also be used to prepare diversified valuable chemical products especially esters and lower olefins.[9] Furthermore, it can be utilized in several fields, for example, in fuel additives of diesel, home heating and cooking gas, and pro-environmental refrigerants.[10,11]

The hydrogenation of CO$_2$ to DME over a hybrid catalyst for DME synthesis is principally composed of three independent reactions, methanol synthesis from CO$_2$ hydrogenation (CO$_2$ + 3H$_2$ $\leftrightarrow$ CH$_3$OH + H$_2$O reaction 1), methanol dehydration to form DME (2CH$_3$OH $\leftrightarrow$ CH$_3$OCH$_3$ + H$_2$O reaction 2), and a reverse water gas shift reaction (RWGS) (CO$_2$ + H$_2$ $\leftrightarrow$ CO + H$_2$O reaction 3). DME can be produced *via* a two-step process including reaction 1 on a copper based catalyst and subsequent

reaction 2 over a solid acid catalyst. Furthermore, one-step process (performing the two steps simultaneously over a hybrid catalyst) has a better performance as a thermodynamically favorable course because the equilibrium limitation of reaction 1 can be readily overcame by reaction 2.[12,13]

Currently, hybrid catalysts of methanol synthesis component and methanol dehydration component are applied to the one-step direct DME synthesis from CO$_2$.[14,15] The methanol dehydration components are generally solid acid catalyst such as γ-Al$_2$O$_3$, but the active sites of the γ-Al$_2$O$_3$ is Lewis acid sites which are favored for water adsorption, resulting in a significant reduction of the amount of acid sites and then a decrease of catalytic activity. Another intriguing solid acid catalyst is WO$_x$/ZrO$_2$, but the catalytic activity of WO$_x$/ZrO$_2$ is lower due to its weaker acid strength present.[16] Besides, SAPO-18 has been used as acid function owing to its uniform microporous structure and a high stability, but SAPO-18 possesses a large number of moderate strength acid sites, which cause catalyst deactivation as well as undesired products by coke deposition.[17] By contrast, HZSM-5 is the most suitable acidic component due to its more hydrophobic character and advantage of Brønsted acidity, which significantly reduces the impact of water on HZSM-5.[18–23] Furthermore, HZSM-5 possesses weak acid sites which are in favor of methanol dehydration to DME at low temperatures and exhibits high catalytic activity.[24] However, the methanol synthesis components of the hybrid catalysts are various, and the Cu–Zn based catalyst is regarded as the most promising binary catalyst among them. Xiao *et al.* reported the deposition of Zn on the surface of copper can increase surface area and can form a unique site at the Cu–ZnO interface to improve the

College of Chemical Engineering, Shenyang University of Chemical Technology, Shenyang 110142, PR China. E-mail: yjzhang2009@163.com; angle_79@163.com; Tel: +86-24-89383902

adsorption of CO_2 and catalyst activity.[25,26] To further improve the performance of the Cu–Zn bimetallic compound catalyst, adding an amphoteric metal oxide species as additive to Cu–Zn based catalyst is an efficient method. Al_2O_3 is a prospective co-catalyst of sufficient attraction due to its mechanical and thermal stability, its excellent dispersion feature of copper and zinc. Nevertheless, only a few literatures have reported Al_2O_3 as a single additive of the Cu–Zn based catalyst for one-step direct DME synthesis from CO_2 hydrogenation at present. Lei *et al.* studied hydrogenation of CO_2 to CH_3OH over CuO–ZnO–Al_2O_3 catalysts prepared *via* a solvent-free route, they found that the combustion processes and physicochemical properties of catalysts depend strongly on the type and amount of fuel.[27] Allahyari *et al.* reported CuO–ZnO–Al_2O_3/HZSM-5 nanocatalyst for direct synthesis DME as a green fuel from syngas, the catalysts were prepared by ultrasound-assisted co-precipitation method at different irradiation times, and the result revealed the relationship between irradiation time and catalytic performance.[28] Bowker *et al.* studied the mechanism of methanol synthesis on copper/zinc oxide/aluminum catalyst, and found that the energetics of formate hydrogenation/hydrogenolysis on the copper component of the catalyst was unaffected by the intimate mixing of copper and zinc oxide in the catalyst.[29] Liu reported preparation of HZSM-5 membrane packed CuO–ZnO–Al_2O_3 nanoparticles for catalysing carbon dioxide hydrogenation to DME, they found zeolite capsule catalysts exhibited an excellent DME selectivity compared with the conventional hybrid catalyst because the further dehydration of DME was restrained.[10] Unfortunately, those above mentioned literature of CO_2 hydrogenation over CuO–ZnO–Al_2O_3 catalyst were mainly related to the influence of catalyst preparation methods to the catalyst activity as well as the mechanism of CO_2 hydrogenation. On the contrary, the effect of the amount of the additive Al_2O_3 of CuO–ZnO–Al_2O_3 catalyst on catalyst activity was rarely investigated. Meanwhile, the Cu/Zn ratio of the CuO–ZnO–Al_2O_3 catalyst currently still derived from methanol synthesis from CO_2 hydrogenation or from syngas hydrogenation.[30]

Here, we prepared a series of CuO–ZnO–Al_2O_3/HZSM-5 hybrid catalysts of different Al_2O_3 contents by the oxalate co-precipitation method, on the basis of optimizing Cu/Zn ratio of catalyst for DME synthesis from CO_2 hydrogenation. The effect of Al_2O_3 content on catalytic properties especially CO_2 conversion and DME selectivity of the hybrid catalysts was investigated. Moreover, the influence of reaction temperature and velocity on the catalyst activity of the hybrid catalyst with optimum Al_2O_3 content was also investigated.

2. Experimental

2.1 Preparation of CuO–ZnO/HZSM-5 catalysts

A series of CuO–ZnO/HZSM-5 catalysts of diverse Cu/Zn molar ratio were prepared, aiming at confirming optimum composition. $Cu(NO_3)_2 \cdot 3H_2O$, $Zn(NO_3)_2 \cdot 6H_2O$ (Cu/Zn molar ratio ranging from 2 : 8 to 8 : 2) were dissolved in ethanol to gain the metal nitrates solution and coprecipitated by oxalate under vigorous stirring at 60 °C in a solution containing the HZSM-5 finely dispersed, with a final CuO–ZnO : HZSM-5 weight ratio

of 2 : 1, for convenience of comparison with previous work.[7,31,32] The HZSM-5 with a SiO_2/Al_2O_3 ratio of 38 was purchased from Catalyst Plant of Nankai University (China). The slurry was heated to 80 °C and was aged for 2 h under stirring. Subsequently, the slurry was evaporated at the same temperature. Then the obtained product was dried in muffler furnace at 120 °C for 12 h and calcined in air at 400 °C for 4 h. The final product was hybrid catalyst named as $C_xZ_{10-x}H$ (the *x* express the molar ratio of CuO : CuO–ZnO) and was pressed, crushed and griddled to get the granules (20–40 mesh).

2.2 Preparation of CuO–ZnO–Al₂O₃/HZSM-5 hybrid catalysts

Thereafter, a series of CuO–ZnO–Al_2O_3/HZSM-5 hybrid catalysts of different Al_2O_3 contents were prepared. $Cu(NO_3)_2 \cdot 3H_2O$, $Zn(NO_3)_2 \cdot 6H_2O$ were weighed according to the optimal Cu/Zn mole ratio which was determined in the preliminary experiments. The mixture was dissolved in ethanol followed by the addition of $Al(NO_3)_2 \cdot 9H_2O$. The amount of the $Al(NO_3)_2 \cdot 9H_2O$ used depended on the required Al_2O_3 contents of 0, 1.0, 3.0, 5.0, 7.0, 10.0 wt% in CuO–ZnO–Al_2O_3. Then, the solution of precursors was added to a vigorously stirred ethanol solution containing the oxalic acid and the powdered HZSM-5 in a constant and slow manner at 60 °C. The weight ratio of the final oxide of CuO–ZnO–Al_2O_3 to HZSM-5 is 2 : 1. The slurry was dealt with the same procedure as the $C_xZ_{10-x}H$ and the final product was abbreviated as CZA_yH, where the *y* represents theoretical Al_2O_3 : CuO–ZnO–Al_2O_3 wt%.

2.3 Catalyst testing

The hybrid catalyst activity was measured in a continuous-flow fixed-bed reactor made of stainless steel (10 mm inner diameter). 1 mL of the hybrid catalyst was diluted with 0.5 mL of the quartz sand (both in 20–40 mesh). Prior to the test, the catalyst was reduced *in situ* in a stream of 10% H_2/N_2 at 300 °C for 3 h under atmospheric pressure. After the reduction, the reactor was cooled to room temperature under flowing N_2 and reactant gas flow ($H_2/CO_2/N_2$ = 3/9/1, molar) was introduced, subsequently raising the pressure to 3.0 MPa and the reaction temperature was raised to 260 °C. Analysis of the products were performed applied a gas chromatograph (SP2100A) equipped with both a TCD (for N_2, CO and CO_2, GDX-101 connected with Porapak T column) and a FID (for CH_4, CH_3OH and DME, Porapak Q column). The CO_2 conversion as well as the selectivity toward CO, CH_3OH and DME are calculated by internal standard method.[32,33] X_{CO_2}, S_{P_i} and Y_{DME} represent the conversion of CO_2, the selectivity of the product (DME, MeOH, CO) and the yield of DME, respectively. Each experimental data was corresponds to an average of three independent measurements, with error of ±2%.

$$X_{CO_2} = \frac{CO_{2,in}/N_{2,in} - CO_{2,out}/N_{2,out}}{CO_{2,in}/N_{2,in}} \quad (1)$$

$$S_{P_i} = \frac{P_i}{1 - CO_{2,out}} \quad (2)$$

where P_i stands for the concentration of a specific i product (DME, MeOH, CO).

$$Y_{DME} = S_{DME} X_{CO_2} \qquad (3)$$

2.4 Catalyst characterization

X-ray powder diffraction (XRD) patterns of all samples were performed on a Rigaku D/max 2500 pc X-ray diffractometer with Cu-Kα radiation ($\lambda = 1.54156$ Å) at a scan rate of $4°$ min^{-1} at 50 kV and 250 mA.

The BET surface area of the samples were conducted by N_2 adsorption at -196 °C using a Quantachrome Autosorb 1-C. Before the absorption–desorption measurements, samples were degassed under vacuum at 300 °C for 3 h. The specific BET (S_{BET}) was estimated from the linear part of the Brunauer–Emmett–Teller (BET) plot.

The X-ray photoelectron spectroscopy (XPS) and X-ray-induced Auger electron spectroscopy were recorded on an ESCALA 250 Xi spectrometer, using a standard Al-Kα X-ray source (1486.6 eV). The binding energy (BE) values were referenced to the adventitious C 1s peak (284.6 eV). Quantification of the surface atomic concentrations was carried out using the sensitivity factors supplied for the XPS instrument.

H_2-TPR of catalysts were performed on chemisorptions (ChemBET 3000). Before reduction, 0.02 g of sample was preheated with flowing He at 400 °C for 60 min, then cooled down room temperature. Subsequently, the temperature was raised in 10% H_2/Ar (50 mL min^{-1}) at a ramp rate of 10 °C min to 400 °C. H_2 consumption was detected by TCD.

NH_3-TPD of the samples were measured on the same apparatus for H_2-TPR measurements. 0.1 g sample was heated to 400 °C and maintained for 30 min, then the temperature was cooled to 100 °C. After that, a 6 vol% NH_3/Ar mixture stream was introduced to the sample for 60 min. Then, the examined sample was flushed with helium stream (30 mL min^{-1}) for 60 min to remove the weak adsorbed NH_3. The temperature was raised from 100 °C to 800 °C at a rate of 10 °C min.

3. Results and discussion

3.1 The effect of the Cu/Zn molar ratio on the catalytic performance of $C_xZ_{10-x}H$ catalysts

In order to investigate the optimal Cu/Zn molar ratio of the hybrid catalysts, a series of $C_xZ_{10-x}H$ catalysts were prepared. The catalytic performances of catalysts with different Cu/Zn molar ratio were summarized in Table 1. The CO_2 conversion, DME selectivity and the yield of DME increased with the Cu/Zn increased from 2 : 8 to 7 : 3, and decreased if continue raising the Cu/Zn to 8 : 2. The C_7Z_3H exhibited the maximum CO_2 conversion, DME selectivity and DME yield values of 19.2%, 47.8% and 9.2%, respectively. The result revealed the Cu/Zn molar ratio can affect the catalytic performance and the optimal Cu/Zn molar ratio of the hybrid catalysts was 7 : 3.

Table 1 Catalytic performance of the $C_xZ_{10-x}H$ Hybrid catalysts[a]

Catalyst	Conversion of CO_2/%	Selectivity/%				Yield/% DME
		DME	CH_3OH	CO	Hydrocarbons	
C_2Z_8H	16.06	25.41	5.34	67.35	1.90	4.08
C_3Z_7H	16.44	27.04	8.03	63.14	1.79	4.45
C_4Z_6H	17.71	36.71	5.23	56.16	1.90	6.50
C_5Z_5H	17.46	37.73	5.22	55.22	1.83	6.59
C_6Z_4H	18.06	38.42	6.01	53.70	1.87	6.94
C_7Z_3H	19.20	47.80	1.70	47.80	2.70	9.20
C_8Z_2H	18.16	39.35	5.15	53.49	2.01	7.15

[a] Reaction conditions: $T = 260$ °C; $P = 3.0$ MPa; $CO_2 : H_2 : N_2 = 3 : 9 : 1$; GHSV = 1500 h^{-1}.

3.2 Catalytic performance of the CZA_yH catalysts

The catalytic performances of the CZA_yH catalysts with different Al_2O_3 contents were listed in Table 2. DME was the major product and the by products included CO and methanol under the reaction temperature of 260 °C, pressure of 3.0 MPa and GHSV of 1500 h^{-1}. Moreover, several hydrocarbons such as CH_4 were also detected. The catalytic performances of the Al_2O_3-modified hybrid catalysts were enhanced enormously compared with the Al_2O_3-free hybrid catalyst. With the Al_2O_3 contents increase in the catalysts (range from CZA_0H to CZA_7H), the CO_2 conversion, DME selectivity and the DME yield increased significantly. Further increasing the contents of Al_2O_3 ($CZA_{10}H$) decreased the catalysts activity. The CZA_7H catalyst exhibited the highest catalyst performance and a maximum CO_2 conversion of 27.3% with a DME selectivity of 67.1% and a yield of DME of 18.3%, as shown in Table 2. The DME yield and the DME selectivity of CZA_7H catalyst were appreciable in comparison of nearly 13.5% and 63.4%, respectively, obtained over CuO–ZnO–ZrO_2/HZSM-5 catalyst reported by Li et al.[34] Meanwhile, the DME selectivity of 67.1% for CZA_7H catalyst was significantly higher than 49.2% observed over CuO–ZnO–Al_2O_3/HZSM-5 catalyst studied by Zhang et al.[31] These results indicated suitable Al_2O_3 additive can improve the catalyst performance significantly.

Fig. 1 shows the effect of reaction temperature on the catalytic performance of CZA_7H catalyst. It can be found that volcanic shape change trends of the CO_2 conversion, DME selectivity and the yield of DME versus the variation of the

Table 2 Catalytic performance of the CZA_yH hybrid catalysts[a]

Catalyst	Conversion of CO_2/%	Selectivity/%				Yield/% DME
		DME	CH_3OH	CO	Hydrocarbons	
CZA_0H	19.2	47.8	1.7	47.8	2.7	9.2
CZA_1H	23.6	60.6	2.0	34.6	2.8	14.3
CZA_3H	22.9	61.6	2.6	33.1	2.7	14.1
CZA_5H	23.0	64.3	5.5	26.5	3.7	14.8
CZA_7H	27.3	67.1	3.9	25.5	3.5	18.3
$CZA_{10}H$	22.6	60.9	3.6	32.7	2.8	13.8

[a] Reaction conditions: $T = 260$ °C; $P = 3.0$ MPa; $CO_2 : H_2 : N_2 = 3 : 9 : 1$; GHSV = 1500 h^{-1}.
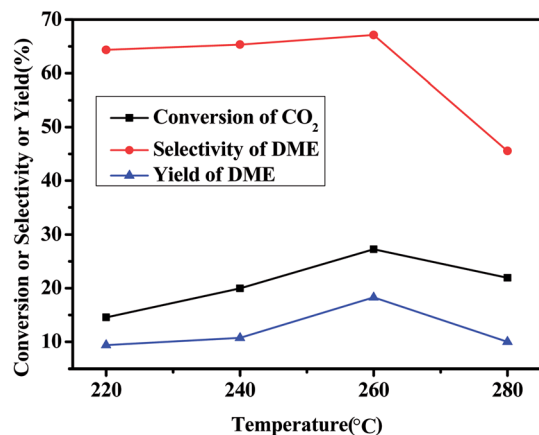
Fig. 1 Effect of temperature on catalytic CO_2 hydrogenation to DME for CZA$_7$H hybrid catalysts.

Fig. 3 Effects of the conversion of CO_2 and the selectivity of DME with CZA$_7$H hybrid catalysts with time on stream.

temperature. With the temperature rising from 220 °C to 260 °C, the conversion of CO_2, the selectivity of the DME and the DME yield increased obviously 12.7%, 2.7% and 8.9%, respectively, and then reduced sharply when the reaction temperature reached 280 °C. Comparing the catalytic performance data at several reaction temperatures, the optimal catalytic performance for the CZA$_7$H catalyst were obtained at 260 °C. These results can be explained by the hydrogenation of CO_2 for synthesis of DME was a reversible exothermic reaction, the reverse reaction favored with an excessive temperature. Meanwhile, the main side reaction RWGS was an endothermic reaction thus the CO selectivity increased and the selectivity and yield of DME decreased with the reaction temperature higher than 260 °C.[5] In addition, the CZA$_7$H catalyst activity may also decrease due to the Cu sintered and crystallized gradually with the reaction temperature increased.[18]

Fig. 2 illustrates the influence of the space velocity of on the catalytic performance of the CZA$_7$H catalyst. It can be found that the CO_2 conversion, the DME selectivity and the DME yield decreased continuously from 27.3% to 20.5%, 67.1% to 52.3% and 18.3% to 10.7%, respectively, as the space velocity increased from 1500 to 3000 h^{-1}. With the space velocity increasing, the
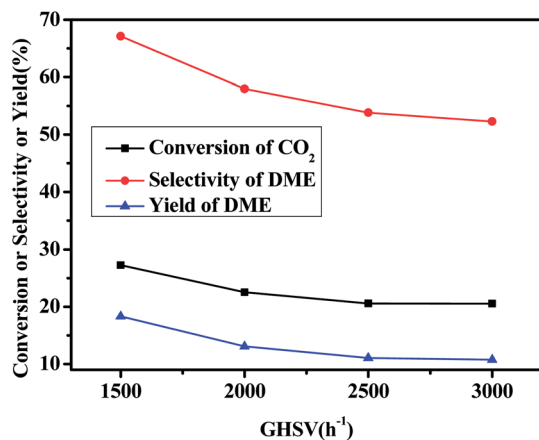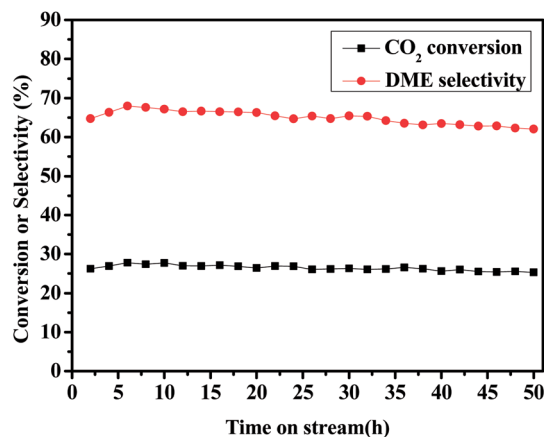
contact time between reactants and the catalyst becomes short, consequently both the CO_2 hydrogenation to methanol and methanol dehydration to DME reactions could not proceed sufficiently.[18] Therefore, the conversion of CO_2 and the selectivity of the DME reduced distinctly indicating the efficient effect the space velocity on the catalytic performance.

3.3 Stability of the CZA$_7$H catalyst

The stability of CZA$_7$H catalyst was studied for the reaction of DME synthesis *via* CO_2 hydrogenation at 260 °C and 3.0 MPa with GHSV = 1500 h^{-1}. The stability results were recorded every 2 h, as shown in Fig. 3. It can be found that the CO_2 conversion of and the DME selectivity decrease slightly from 27.3% and 67.1% to 25.3% and 62.1% during the continuous 50 h reaction process, respectively. The result indicated that the CZA$_7$H catalyst possessed better catalytic performance and stability.

3.4 The structure of the catalysts

Fig. 4 illustrates the XRD patterns of a series of CZA$_y$H catalysts with different Al_2O_3 contents before H_2 reduction. For all catalysts, the diffraction peaks at $2\theta = 35.5°, 38.7°, 48.7°, 53.4°, 58.2°, 61.5°, 66.2°, 72.3°$ and $74.9°$ can be ascribed to CuO phase (JCPDS no. 48-1548), the peaks at $2\theta = 31.7°, 34.3°, 36.1°, 47.4°, 56.5°, 62.8°$ and $67.8°$ can be attributed to ZnO phase (JCPDS no. 65-3411), and the peaks appear in the 2θ range of 21–25° can be matched to HZSM-5 (JCPDS no. 44-0003). The peaks corresponding to Al_2O_3 phase cannot be observed, indicating that the presence of Al_2O_3 were amorphous phase or highly dispersed in the catalyst body phase. Compared with the peaks of catalyst CZA$_0$H, the peaks of catalysts with Al_2O_3 become weaker, indicating the CuO–ZnO oxides possess less intensive crystallinity. The diffraction peaks of CuO and ZnO weakened and broadened gradually with the increasing of Al_2O_3 contents, even some diffraction peaks of CuO and ZnO phase disappeared, suggesting the decrease of grain size. The grain sizes of CuO (d_{CuO}) and ZnO (d_{ZnO}) for CZA$_x$H catalysts calculated by Scherrer's equation are listed in Table 3. These results indicated obviously that the additive of Al_2O_3 can improve the CuO dispersion and
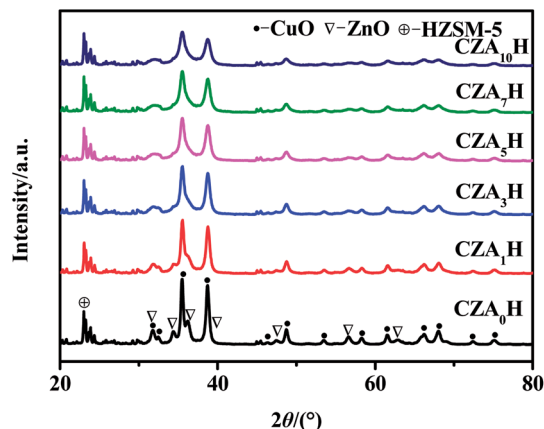

Fig. 2 Effect of space velocity on catalytic CO_2 hydrogenation to DME for CZA$_7$H hybrid catalysts.

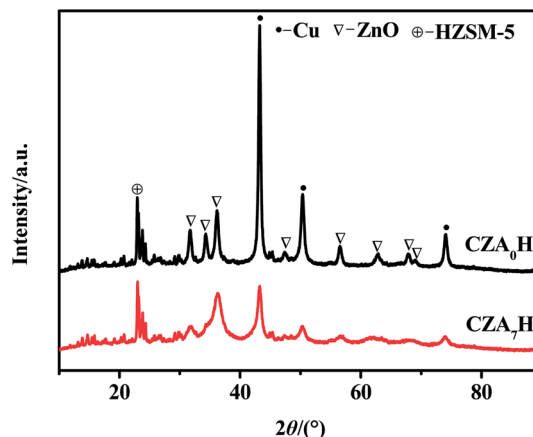Fig. 4 XRD patterns of the CZA$_y$H hybrid catalysts.

Fig. 5 XRD patterns of the reduced CZA$_0$H and CZA$_7$H hybrid catalysts.

can decrease the grain size of CuO. For all catalysts, the grain size of ZnO phase is greater than that of CuO phase, indicating ZnO phase closely relates to CuO phase. Shimokawabe *et al.* considered the grain size of ZnO is larger than CuO due to CuO can be well dissolved on the ZnO particles.[35] As a consequence, the active interface increased with the improving the dispersion of CuO.[35,36] Fig. 5 shows the XRD patterns of the reduced CZA$_0$H and CZA$_7$H catalysts. For these two catalysts, the diffraction peaks at 2θ = 43.3°, 50.4° and 74.1° can be ascribed to metallic copper phase (JCPDS no. 04-0836). No diffraction peaks of CuO can be detected, indicating all CuO in the catalysts reduced to Cu. The intensity of diffraction peaks of Cu for reduced CZA$_7$H catalyst decrease significantly, compared to the corresponding peaks for CZA$_0$H catalyst. Furthermore, the grain size of Cu decreased significantly for CZA$_7$H catalyst. As shown in Table 3, and the grain sizes of Cu (d_{Cu}) which calculated by Scherrer's equation for reduced CZA$_0$H and CZA$_7$H are 21.4 nm and 9.7 nm, respectively. These results suggest that the addition of Al$_2$O$_3$ can effectively inhibit the Cu crystals growth.

The BET Surface areas (S_{BET}) and the calculated average pore diameter of the catalysts are also listed in Table 3. The S_{BET} of the catalysts approximately increases from 131.7 m^2 g^{-1} to 161.2 m^2 g^{-1} with the increasing of Al$_2$O$_3$ contents (from CZA$_0$H to CZA$_7$H), then sharply decreases to 143.5 m^2 g^{-1} when the Al$_2$O$_3$ contents continuing increasing (CZA$_{10}$H). The variation trend of the micropore volumes is the same as the S_{BET} while the trend of average pore diameter of the catalysts is contrary to the S_{BET}

generally. These results illustrate that the pore structure of the hybrid catalysts can be changed by the introduction of Al$_2$O$_3$. Meanwhile, a maximum S_{BET} of 161.2 m^2 g^{-1} and a minimum average pore diameter of 6.8 nm are detected for the CZA$_7$H catalyst which possesses the smallest grain sizes of Cu (d_{Cu}), as determined from XRD. The result revealed that why the catalyst of CZA$_7$H exhibited the maximum of the CO$_2$ conversion, the DME selectivity and the DME yield simultaneously.

3.5 The reducibility of the catalysts

TPR measurements were carried out in order to evaluate the reduction behavior of all the catalysts. Fig. 6 shows the H$_2$-TPR profiles of the CZA$_x$H catalysts with different Al$_2$O$_3$ contents. It can be found only a single reduction peak with any satellite peaks for all the catalysts. The result illustrate the opinion the copper oxides on the CZA$_x$H catalysts are easy to be reduced.[37] Since ZnO and Al$_2$O$_3$ cannot be reduced under the experimental condition, the single high temperature reduction peak can be ascribed to the reduction of CuO species with strongly interaction with ZnO and Al$_2$O$_3$.[38] With Al$_2$O$_3$ content increasing, the reduction peak maximum firstly shifted towards higher temperature from CZA$_0$H to CZA$_7$H catalysts, and then shifted towards lower temperature for CZA$_{10}$H, as shown in Fig. 6. The CZA$_7$H catalyst possessed the highest reduction temperature at 373 °C, which indicated the strongest interaction between the

Table 3 Physicochemical properties of the CZA$_y$H hybrid catalysts

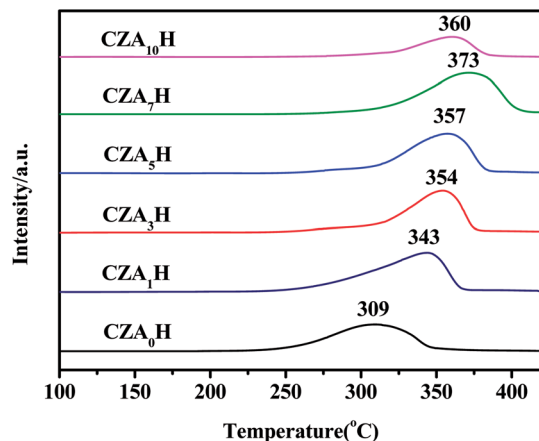| Catalyst	S_{BET}/(m^2 g^{-1})	V_1 (Micropore volume)/(cm^3 g^{-1})	D (Average pore diameter)/nm	$d_{CuO}{}^a$/nm	$d_{Cu}{}^a$/nm	$d_{ZnO}{}^a$/nm
CZA$_0$H	131.7	0.032	8.0	20.4	21.4	29.1
CZA$_1$H	132.1	0.024	8.7	15.4	—	17.6
CZA$_3$H	133.4	0.028	7.7	14.4	—	16.5
CZA$_5$H	134.1	0.031	7.6	11.4	—	14.1
CZA$_7$H	161.2	0.037	6.8	10.9	9.7	13.4
CZA$_{10}$H	143.5	0.030	7.6	10.6	—	12.3

^{a} Determined by Scherrer's equation.

Fig. 6 H_2-TPR profiles of the CZA_yH hybrid catalysts.

Table 4 The reduction peak areas of the CZA_yH hybrid catalysts

Catalyst	CZA_0H	CZA_1H	CZA_3H	CZA_5H	CZA_7H	$CZA_{10}H$
Peak area	25 065	30 247	26 320	32 048	38 894	15 425

heterogeneous CuO particles with metal oxides. The CZA_7H catalyst exhibited the best catalytic performance which might be explained that strongly interaction between CuO and oxides was beneficial to CO_2 hydrogenation to DME.[39] Meanwhile, the CZA_7H catalyst possessed the largest area among the reducing peaks, which revealed that the hydrogen consumption of the catalyst was enhanced significantly, as shown in Table 4. The result implied the largest amount of easily reducible well-dispersed copper oxide existed, which might also be ascribed to the improving dispersion of the CuO particles.[40] This may be one reason why when increase Al_2O_3 contents in the catalysts from CZA_0H to CZA_7H, the conversion and selectivity significantly increased and a further increase in Al_2O_3 contents adversely influenced conversion and selectivity simultaneously.

3.6 Surface acidity of the CuO–ZnO–Al₂O₃/HZSM-5 catalysts

Fig. 7 shows NH_3-TPD profiles of the CZA_xH catalysts with different Al_2O_3 contents. It can be found three NH_3 desorption peaks which located in the range of 50–200 °C (denoted as peak α), 200–350 °C (denoted as peak β), and 350–600 °C (denoted as peak γ), respectively. The α, β and γ peaks were attributed to weak, medium and strong acid sites, respectively, indicating the presence of three strength acid sites on the hybrid catalysts.[33] The intensity of the low-temperature peak α of weak acid sites firstly increased with increasing Al_2O_3 contents (from CZA_0H to CZA_7H) and then declined with further increasing Al_2O_3 additive, which was agreement with the trend of S_{BET} and H_2-TPR. The CZA_7H catalyst of the highest peak intensity possessed the largest amount of weak acid sites which were beneficial for methanol dehydration to DME at low temperatures.[24] This might be ascribed to the fact Al_2O_3 owned weak acidic characters. In addition, the intensity and the position of the peaks
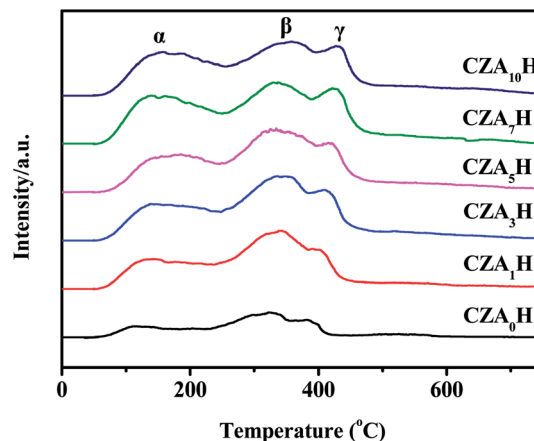

Fig. 7 NH_3-TPD profiles of the CZA_yH hybrid catalysts.

β exhibited unconspicuous changes with doping different Al_2O_3 contents, implying that the strength and amount of medium acid sites cannot be influenced by Al_2O_3 additive substantially. The position of peaks γ shifted towards higher temperature gradually, indicating the intensity of strong acid sites increased with increasing Al_2O_3 doping, leading to the increase of hydrocarbons in the products. This might be attributed to the fact that the HZSM-5 with possessed strong acid sites could be modified by more oxalic acid with the addition of the more Al_2O_3 contents, during the preparation of hybrid catalysts by the co-precipitation method.[11,34] From the above, the amount of weak acid sites enhanced with optimal Al_2O_3 modified, which was in favor of obtaining the highest catalytic performance for one-step DME synthesis reaction.[24]

3.7 XPS analysis

The XPS spectra of reduced catalysts are shown in Fig. 8. Both of the spectra contained two peaks at about 1022 and 1045 eV (Fig. 8a), which were assigned to Zn $2p_{3/2}$ and Zn $2p_{1/2}$ peaks of ZnO, respectively, with a spin energy separation of 23 eV.[41] This illustrates that the Zn atoms are in a completely oxidized state and were not reduced.[42] It can be observed a single peak centered at near 74.2 eV in Fig. 8b, which was attributed to Al $2p_{3/2}$ of Al_2O_3, therefore, the form of Al was Al_2O_3. Fig. 8c showed the XPS spectra of the Cu 2p for the reduced CZA_0H and CZA_7H catalysts. Two reduced catalysts displayed Cu $2p_{3/2}$ and Cu $2p_{1/2}$ main characteristics peaks with binding energy (BE) values of approximately 932.6 eV and 952.6 eV, respectively, with a Cu 2p core level split spin–orbit components (ΔCu 2p) of 20.0 eV. The shake-up satellite peaks between 940 eV and 945 eV were not detected, which illustrates the absence of Cu^{2+} species in both CZA_0H and CZA_7H catalysts can be reduced to Cu^+ and/or Cu^0 species completely.[43,44] Meanwhile, the binding energy (BE) of Cu $2p_{3/2}$ and Cu $2p_{1/2}$ for reduced CZA_7H can be observed slightly shifted towards lower BE values, which revealed an enhancement on the interaction between Cu and ZnO with the increasing Al_2O_3 contents.[45] The result indicated an influence on Cu chemical combination state due to the increase of the outer-shell electron density of Cu as a consequence of the introduction of additive Al_2O_3. Liu *et al.* thought that the
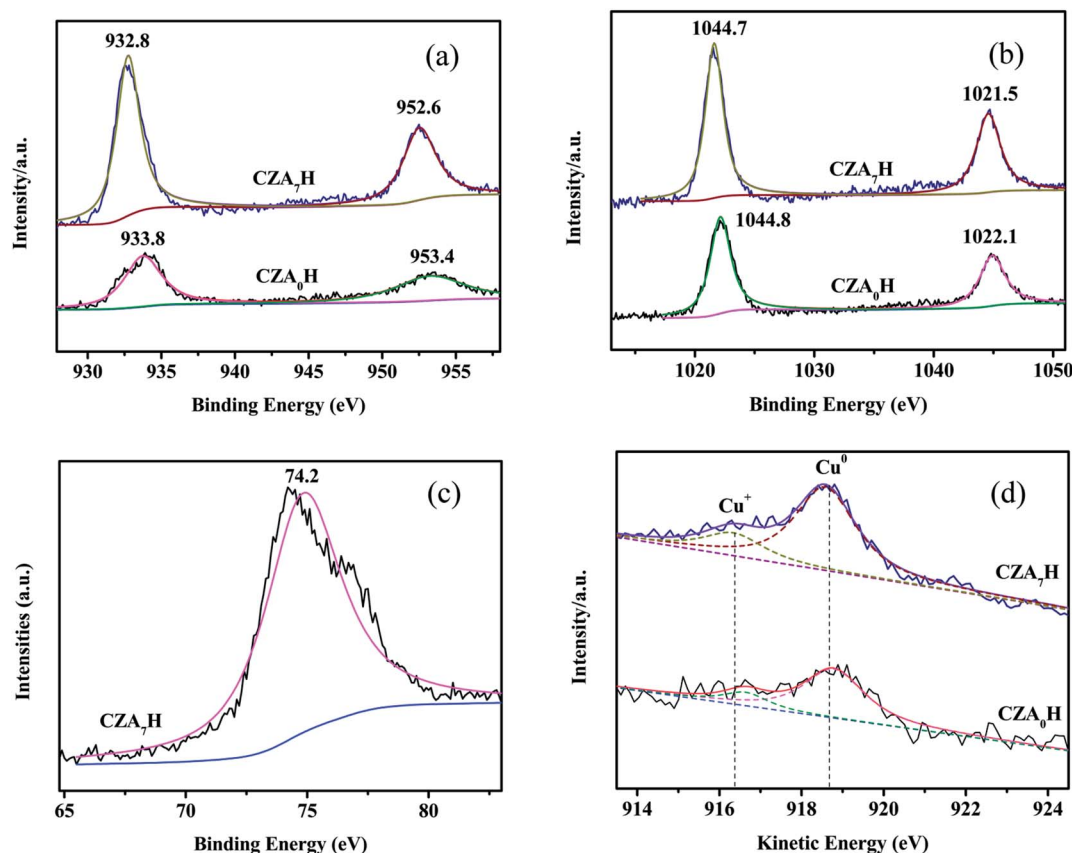
Fig. 8 Spectra of the reduced CZA_0H and CZA_7H hybrid catalysts: (a) Cu 2p; (b) Zn 2p; (c) Al 2p; (d) Cu (LMM) Auger.

chemical state of Cu was tightly related to the catalysts performance for CO_2 hydrogenation to DME.[46] This point might be one reason answerable for doping Al_2O_3 affect the activity of the hybrid catalysts. To distinguish Cu^+ and Cu^0 species, the kinetic energies (KE) of the Cu LMM X-ray auger electron spectroscopy (XAES) spectrum are measured. As shown in Fig. 8d, a broad and asymmetric peak was divided into two peaks, which centered at near 916.5 and 918.7 eV for both reduced CZA_0H and CZA_7H catalysts. The two symmetrical peaks are corresponding to the Cu^+ and Cu^0 species, respectively. The line position in the Cu LMM Auger electron spectrum of the two reduced catalysts illustrated that the Cu^0 was the predominant copper species on the CZA_0H and CZA_7H catalysts surface. Furthermore, the Cu^0/Cu^+ area ratios of the two reduced catalysts were calculated based on the corresponding Cu LMM peaks. The area ratio of the reduced CZA_7H catalyst is a bit higher than that of the CZA_0H catalyst, which indicated that Cu^0 species but not Cu^+ species might in charge of the activity of these catalysts.[47] The result might be another reason responsible for the improvement in catalytic performance for the Al_2O_3-modified hybrid catalysts.[48,49]
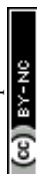
properties and catalytic performance of the hybrid catalysts based on the optimizing Cu/Zn ratio. The hybrid catalysts for the reaction of CO_2 directly hydrogenation to DME improved the CuO dispersion, reduced the CuO crystallite size, decreased the grain size of the Cu, enhanced the BET surface areas, increased the interaction between the CuO and ZnO, enhanced the amount of weak acid sites, changed the copper chemical state on the catalysts surface and enhanced the catalytic activity and stability with the introduction of the Al_2O_3 contents. In addition, the influence of the reaction temperature and the space velocity on the catalytic performance of the catalysts modified by Al_2O_3 was also investigated. The optimal Al_2O_3 contents (Al_2O_3 : CuO–ZnO–Al_2O_3 wt%) of the CuO–ZnO–Al_2O_3/HZSM-5 catalysts was 7.0 wt% under the proper Cu/Zn ratio of 7 : 3. The CZA_7H catalyst for CO_2 hydrogenation to DME showed the maximum CO_2 conversion, DME selectivity and DME yield of 27.3%, 67.1% and 18.3%, respectively, under the reaction conditions of the optimal reaction temperature 260 °C, the appropriate space velocity of GHSV 1500 h^{-1} and the conventional pressure of 3.0 MPa.

4. Conclusions

The work discussed the effect of the amount of Al_2O_3 additive of the CuO–ZnO–Al_2O_3/HZSM-5 catalysts on the physicochemical

Conflicts of interest

There are no conflicts to declare.

Acknowledgements

References

1 T. Witoon, T. Permsirivanich, N. Kanjanasoontorn, C. Akkaraphataworn, A. Seubsai, K. Faungnawakij, C. Warakulwit, M. Chareonpanich and J. Limtrakul, *Catal. Sci. Technol.*, 2015, **5**, 2347–2357.

2 T. Phongamwong, U. Chantaprasertporn, T. Witoon, T. Numpilai, Y. Poo-arporn, W. Limphirat, W. Donphai, P. Dittanet, M. Chareonpanich and J. Limtraku, *Chem. Eng. J.*, 2017, **316**, 692–703.

3 T. Witoon, N. Kachaban, W. Donphai, P. Kidkhunthod, K. Faungnawakij, M. Chareonpanich and J. Limtraku, *Energy Convers. Manage.*, 2016, **118**, 21–31.

4 T. Witoon, S. Bumrungsalee, M. Chareonpanich and J. Limtraku, *Energy Convers. Manage.*, 2015, **103**, 886–894.

5 K. H. Sun, Z. G. Fan, J. Y. Ye, J. M. Yan, Q. F. Ge, Y. N. Li, W. J. He, W. M. Yang and C. J. Liu, *Journal of CO₂ Utilization*, 2015, **12**, 1–6.

6 R. J. da Silva, A. F. Pimentel, R. S. Monteiro and C. J. A. Mota, *Journal of CO₂ Utilization*, 2016, **15**, 83–88.

7 G. Bonura, C. Cannilla, L. Frusteri, A. Mezzapica and F. Frusteri, *Catal. Today*, 2017, **281**, 337–344.

8 Y. Suwannapichat, T. Numpilai, N. Chanlek, K. Faungnawakij, M. Chareonpanich, J. Limtraku and T. Witoon, *Energy Convers. Manage.*, 2018, **159**, 20–29.

9 Y. X. Hua, X. M. Guo, D. S. Mao, G. Z. Lu, G. L. Rempel and F. T. T. Ng, *Appl. Catal., A*, 2017, **540**, 68–74.

10 R. Liu, H. F. Tian, A. M. Yang, F. Zha, J. Ding and Y. Chang, *Appl. Surf. Sci.*, 2015, **345**, 1–9.

11 D. S. Mao, J. C. Xia, B. Zhang and G. Z. Lu, *Energy Convers. Manage.*, 2010, **51**, 1134–1139.

12 G. X. Jia, Y. S. Tan and Y. Z. Han, *Ind. Eng. Chem. Res.*, 2006, **45**, 1152–1159.

13 R. Vakili, H. Rahmanifard, P. Maroufi, R. Eslamloueyan and M. R. Rahimpour, *Int. J. Hydrogen Energy*, 2011, **36**, 4354–4365.

14 W. G. Gao, H. Wang, Y. H. Wang, W. Guo and M. Y. Jia, *J. Rare Earths*, 2013, **31**, 470–476.

15 A. García-Trenco and A. Martínez, *Appl. Catal., A*, 2015, **493**, 40–49.

16 T. Witoon, P. Kidkhunthod, M. Chareonpanich and J. Limtrakul, *Chem. Eng. J.*, 2018, **348**, 713–722.

17 A. Ateka, I. Sierra, J. Ereña, J. Bilbao and A. T. Aguayo, *Fuel Process. Technol.*, 2016, **152**, 34–45.

18 X. H. Zhou, T. M. Su, Y. X. Jiang, Z. Z. Qin, H. B. Ji and Z. H. Guo, *Chem. Eng. Sci.*, 2016, **153**, 10–20.

19 A. García-Trenco and A. Martínez, *Appl. Catal., A*, 2012, **411–412**, 170–179.

20 S. Wang, D. S. Mao, X. M. Guo, G. S. Wu and G. Z. Lu, *Catal. Commun.*, 2009, **10**, 1367–1370.

21 T. Takeguchi, K. Yanagisawa, T. Inui and M. Inoue, *Appl. Catal., A*, 2000, **192**, 201–209.

22 V. Vishwanathan, K. W. Jun, J. W. Kim and H. S. Roh, *Appl. Catal., A*, 2004, **276**, 251–255.

23 M. Xu, J. H. Lunsford, D. W. Goodman and A. Bhattacharyya, *Appl. Catal., A*, 1997, **149**, 289–301.

24 Y. J. Lee, M. H. Jung, J. B. Lee, K. E. Jeong, H. S. Roh, Y. W. Suh and J. W. Bae, *Catal. Today*, 2013, **228**, 175–182.

25 J. Xiao, D. S. Mao, X. M. Guo and J. Yu, *Appl. Surf. Sci.*, 2015, **338**, 146–153.

26 J. Toyira, M. Saitob, I. Yamauchic, S. Luoa, J. Wua, I. Takaharab and M. Takeuchid, *Catal. Today*, 1998, **45**, 245–250.

27 H. Lei, Z. Y. Hou and J. W. Xie, *Fuel*, 2016, **164**, 191–198.

28 S. Allahyari, M. Haghighi, A. Ebadi and H. Saeedi, *J. Power Sources*, 2014, **272**, 929–939.

29 M. Bowker, R. A. Hadden, H. Houghton, J. N. K. Hyland and K. C. Waugh, *J. Catal.*, 1988, **109**, 263–273.

30 F. Arena, G. Italiano, K. Barbera, S. Bordiga, G. Bonura, L. Spadaro and F. Frusteri, *Appl. Catal., A*, 2008, **350**, 16–23.

31 Y. J. Zhang, D. B. Li, S. J. Zhang, K. J. Wang and J. Wu, *RSC Adv.*, 2014, **4**, 16391–16396.

32 Y. J. Zhang, Y. Zhang, F. Ding, K. J. Wang, X. L. Wang, B. J. Ren and J. Wu, *Chem. Ind. Chem. Eng. Q.*, 2017, **23**, 49–56.

33 G. Bonura, M. Cordaro, L. Spadaro, C. Cannilla, F. Arena and F. Frusteri, *Appl. Catal., B*, 2013, **140–141**, 16–24.

34 L. Y. Li, D. S. Mao, J. Xiao, L. Li, X. M. Guo and J. Yu, *Chem. Eng. Res. Des.*, 2016, **111**, 100–108.

35 M. Shimokawabe, H. Asakawa and N. Takezawa, *Appl. Catal.*, 1990, **59**, 45–58.

36 L. Shi, C. Y. Zeng, T. J. Wang and N. Tubaki, *Catal. Sci. Technol.*, 2012, **2**, 2569–2577.

37 P. S. Sai Prasad, J. W. Bae, S. H. Kang, Y. J. Lee and K. W. Jun, *Fuel Process. Technol.*, 2008, **89**, 1281–1286.

38 X. M. Guo, D. S. Mao, G. Z. Lu, S. Wang and G. S. Wu, *J. Catal.*, 2010, **271**, 178–185.

39 L. P. Cui, T. Zhou, N. Li, Z. H. Gao, Z. J. Zuo and W. Huang, *Catal. Lett.*, 2017, **147**, 2023–2027.

40 Y. J. Zhang, D. B. Li, Y. Zhang, Y. Cao, S. J. Zhang, K. J. Wang, F. Ding and J. Wu, *Catal. Commun.*, 2014, **55**, 49–52.

41 O. Lupan, G. A. Emelchenko, V. V. Ursaki, G. Chai, A. N. Redkin, A. N. Gruzintsev, I. M. Tiginyanu, L. Chow, L. K. Ono, B. Roldan Cuenya, H. Heinrich and E. E. Yakimov, *Mater. Res. Bull.*, 2010, **45**, 1026–1032.

42 R. Al-Gaashani, S. Radiman, A. R. Daud, N. Tabet and Y. Al-Douri, *Ceram. Int.*, 2013, **39**, 2283–2292.

43 Y. H. Wang, W. G. Gao, H. Wang, Y. E. Zheng, W. Na and K. Z. Li, *RSC Adv.*, 2017, **7**, 8709–8717.

44 Z. Q. Wang, Z. N. Xu, S. Y. Peng, M. J. Zhang, G. Lu, Q. S. Chen, Y. M. Chen and G. C. Guo, *ACS Catal.*, 2015, **5**, 4255–4259.

45 Y. J. Zhao, B. Shan, Y. Wang, J. H. Zhou, S. P. Wang and X. B. Ma, *Ind. Eng. Chem. Res.*, 2018, **57**, 4526–4534.
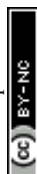
46 R. W. Liu, Z. Z. Qin, H. B. Ji and T. M. Su, *Ind. Eng. Chem. Res.*, 2013, **52**, 16648–16655.

47 P. Gao, L. S. Zhong, L. N. Zhang, H. Wang, N. Zhao, W. Wei and Y. H. Sun, *Catal. Sci. Technol.*, 2015, **5**, 4365–4377.

48 B. Xue, L. Hui, H. Q. Yang, Y. L. Zhao, L. X. Hou and W. Li, *Ind. Eng. Chem. Res.*, 2017, **56**, 135–142.

49 Y. J. Zhang, N. Zheng, K. J. Wang, S. J. Zhang and J. Wu, *J. Nanomater.*, 2013, **7**, 246–247.